Annals of Botany **113**: 105–118, 2014
doi:10.1093/aob/mct262, available online at www.aob.oxfordjournals.org

ANNALS OF BOTANY
Founded 1887

Ontogenetic tissue modification in *Malus* fruit peduncles: the role of sclereids

Melanie Horbens[1,*], Alexander Feldner[2], Monika Höfer[3] and Christoph Neinhuis[1]

[1]*Institute of Botany, Technische Universität Dresden, Zellescher Weg 20b, D-01217 Dresden, Germany,* [2]*Institute of Plant and Wood Chemistry, Technische Universität Dresden, Pienner Strasse 19, D-01737 Tharandt, Germany and* [3]*Julius Kühn-Institute, Federal Research Centre for Cultivated Plants, Institute for Breeding Research on Horticultural and Fruit Crops, Pillnitzer Platz 3a, D-01326 Dresden, Germany*

** For correspondence. E-mail melanie.horbens@tu-dresden.de*

Received: 2 July 2013 Returned for revision: 21 August 2013 Accepted: 20 September 2013 Published electronically: 27 November 2013

• *Background and Aims* Apple (*Malus*) fruit peduncles are highly modified stems with limited secondary growth because fruit ripening lasts only one season. They must reliably connect rather heavy fruits to the branch and cope with increasing fruit weight, which induces dynamic stresses under oscillating wind loads. This study focuses on tissue modification of these small, exposed structures during fruit development.
• *Methods* A combination of microscopic, static and dynamic mechanical tests, as well as Raman spectroscopy, was used to study structure–function relationships in peduncles of one cultivar and 12 wild species, representatively chosen from all sections of the genus *Malus*. Tissue differentiation and ontogenetic changes in mechanical properties of *Malus* peduncles were observed throughout one growing season and after successive removal of tissues.
• *Key Results* Unlike in regular stems, the vascular cambium produces mainly phloem during secondary growth. Hence, in addition to a reduced xylem, all species developed a centrally arranged sclerenchyma ring composed of fibres and brachysclereids. Based on differences in cell-wall thickness, and proportions and arrangement of sclereids, two types of peduncle construction could be distinguished. Fibres provide an increased maximum tensile strength and contribute most to the overall axial rigidity of the peduncles. Sclereids contribute insignificantly to peduncle strength; however, despite being shown to have a lower elastic modulus than fibres, they are the most effective tissue in stiffening peduncles against bending.
• *Conclusions* The experimental data revealed that sclereids originating from cortical parenchyma act as 'accessory' cells to enhance proportions of sclerenchyma during secondary growth in peduncles. The mechanism can be interpreted as an adaptation to continuously increasing fruit loads. Under oscillating longitudinal stresses, sclereids may be regarded as regulating elements between maintenance of stiffness and viscous damping, the latter property being attributed to the cortical parenchyma.

Key words: Apple, biomechanics, fibres, fruit peduncle, fruit load, functional anatomy, *Malus*, sclereids, viscous damping.

INTRODUCTION

Plants are in various ways able to adapt the geometry and material properties of their organs, tissues and cells to changing conditions during development (Niklas, 1992; Burgert and Fratzl, 2009). Trees, for example, form reaction tissues such as compression wood in conifers or tension wood in angiosperms to adjust mechanical properties upon additional weight or external forces by generating longitudinal compressive stresses abaxially, or tensile stresses adaxially, respectively (Burgert *et al.*, 2007; Goswami *et al.*, 2008).

Fruit peduncles and infructescences are highly modified stems with limited secondary growth because fruit ripening lasts only one season or a few months. First, fruit peduncles need to attach fruits to the branch reliably. They also have to adapt to the increasing fruit weight and consequently higher weight force, which induce dynamic stresses under oscillating wind loads. While hanging fruits mainly cause tensile forces, other fruit orientations induce additional bending moments and transverse stresses such as in curved peduncles. Consequently, the question arises whether fruit peduncles show comparable adaptive strategies to branches, especially with large fruit masses. Besides applied aspects in agriculture these processes are of particular interest from the biomechanical or biomimetic perspective. Previous studies on fruit peduncles have focused on (1) the formation of an abscission zone, (2) vascular development or (3) changes in fruit peduncle development against the backdrop of robotic fruit harvesting (Namikawa, 1922; Lang and Ryan, 1994; Drazeta *et al.*, 2004; Sun *et al.*, 2009; Ganino *et al.*, 2011). Only Schwarz (1929) has discussed biomechanical aspects based on anatomical studies and mechanical breaking load tests.

Peduncles and stems of *Kigelia pinnata* (Jaqu.) DC. (Bignoniaceae) and *Couroupita guianensis* Aubl. (Lecythidaceae), which bear fruits weighing 1–5 kg, form reaction wood with gelatinous fibres exhibiting a lumen filled with an additional G-layer (Sivan *et al.*, 2010). This reaction wood consists almost entirely of cellulose microfibrils arranged parallel to the cell axis. During cell differentiation G-fibres tend to contract longitudinally and thus generate considerable longitudinal stresses (Goswami *et al.*, 2008; Mellerowicz *et al.*, 2008). The resulting tension wood is more pronounced in fruit-bearing peduncles than in young inflorescences. Peduncles of *K. pinnata* are about 3·5 m long, hang vertically and develop uniformly distributed G-fibres interpreted

as a response to stress by increasing fruit weight. Fruit peduncles of olive (*Olea europaea* L., Oleaceae) (Ganino *et al.*, 2011), guava (*Psidium guajava* L., Myrtaceae) (Rivero-Maldonado *et al.*, 2008) and some Rosaceae species/cultivars of the genera *Prunus*, *Pyrus* and *Malus* (Schwarz, 1929) share a similar anatomical organization: centrally arranged vascular bundles, a mostly reduced xylem and a partially lignified pith parenchyma. During fruit development, olive peduncles increase their vascular tissue while cells surrounding the phloem differentiate into lignified fibre bundles (Ganino *et al.*, 2011). Olive peduncles lack sclereids in contrast to stems in which they are abundant. Hence, a greater flexibility of peduncles compared with stems was assumed. A histopathological study revealed varying proportions of tissues in guava peduncles depending on fruit size (Rivero-Maldonado *et al.*, 2008). Moreover, the degree of damage by mites correlated with the formation of brachysclereids or phenolic cells within the cortical parenchyma. In addition to fibres, fruit peduncles of some *Malus* and *Pyrus* cultivars develop brachysclereids within the cortical parenchyma (Schwarz, 1929). Sclereids are also abundant in the secondary phloem in *Malus* stems (Evert, 1963). While the proportion of different tissues varies along the peduncle, the maximum volume of strengthening tissue is generally located in the middle (Schwarz, 1929). However, the differing presence and number of sclereids in peduncles has so far not been interpreted.

Sclereids are widespread among higher plants (Evert, 2006; Khatun and Mondal, 2011). Their appearance has been frequently recorded in different plant parts: fruit pericarps (Cai *et al.*, 2010; Romanov *et al.*, 2011), leaves and petioles (Boyd *et al.*, 1982; Heide-Jorgensen, 1990), flowers (Zhang *et al.*, 2010; Reutemann *et al.*, 2012), corms (Bogart *et al.*, 2010), stems (Sharma, 1970; Hernandez-Ladesma *et al.*, 2011), and especially in the bark of trees (Franceschi *et al.*, 2005; Prislan *et al.*, 2012). They often appear at isolated positions and form various, partially bizarre shapes. Most common are isodiametric cells, called brachysclereids or stone cells. Sclereids arise either directly from a meristem or are produced by belated sclerified parenchyma cells (Evert, 2006). Their thick and lignified secondary cell walls show helicoidal structures (Parameswaran, 1975; Roland *et al.*, 1987; Reis and Vian, 2004). Hence, together with fibres sclereids are traditionally classified as sclerenchyma and have been mainly assigned to play a protective role (Eschrich, 1995; Evert, 2006). For example, the outer cylinder of sclerenchymatous fibres in young stems of lianescent *Aristolochia* species disintegrates during secondary growth and the gaps are filled with parenchymatous cells which subsequently differentiate into sclereids. This process has been described as a self-repair mechanism (Busch *et al.*, 2010). Additional functions of sclereids have been described and partly experimentally proven, including (1) light-guidance by foliar sclereids in evergreen sclerophylls (Karabourniotis, 1998), (2) facilitated water conduction through palisade cells to the epidermis by osteosclereids in xeromorphic leaves of *Hakea suaveolens* R. Br. (Proteaceae) (Heide-Jorgensen, 1990) and (3) the reinforcement of *Camellia* (Theaceae) corollas against rainfall by spindle-shaped, monomorphic and polymorphic sclereids (Zhang *et al.*, 2010). However, experimental studies on the specific mechanical advantage of sclereids are generally lacking.

We studied the biomechanics of fruit peduncles in the genus *Malus*, which comprises between 25 and 55 species that are easily accessible and show a large variety in fruit form, size and mass (Robinson *et al.*, 2001; Harris *et al.*, 2002; Höfer *et al.*, 2013). The experimental approach focused on the occurrence, development and mechanics of the strengthening tissues in *Malus* peduncles and addressed the following questions: (1) Which *Malus* species possess sclereids in their peduncles? (2) What is the purpose of the combination of prosenchymatic fibres and isodiametric sclereids? (3) Does the occurrence of brachysclereids constitute an adaptive strategy to increasing fruit weights?

A combination of microscopic and mechanical test methods, as well as Raman spectroscopy was applied to study structure–function relationships in *Malus* peduncles. First, anatomical investigations were accompanied by biomechanical tests under (1) static loads and (2) dynamic oscillation conditions to trace tissue differentiation and ontogenetic changes in elastic and, additionally, viscous properties of *Malus* peduncles throughout the growing season. Second, mechanical investigation of peduncles (static conditions) after successive removal of tissues revealed insights into the specific mechanical properties and function of different tissues.

MATERIAL AND METHODS

Plant material

Developing fruits of 12 *Malus* wild species (rootstock 'Bittenfelder Sämling') from various sections as well as one cultivar (rootstock M 9) (Table 1) were collected in Dresden-Pillnitz, Germany (51°0′32″N, 13°52′27″E), in the fruit gene bank of the Julius Kühn-Institute, Institute for Breeding Research on Horticultural and Fruit Crops as well as in the horticultural test field at the Saxon State Office for Environment, Agriculture and Geology. Sampling comprised 20–40 fruits with at least 20 peduncles from two trees of one to two accessions of each species and stage of development, respectively. Fruits were chosen randomly from trees. Investigations started at the full bloom stage (50 % of flowers open, BBCH-code 65 according to Meier *et al.*, 1994) in spring 2011, and continued during the growing season. Fruits of seven developmental stages were sampled and chosen according to the tissue differentiation in the peduncle. Peduncles used for studies with isolated tissues were collected in September 2012. All samples were kept hydrated at 4 °C for a maximum of 48 h.

Microscopy

Peduncles were fixed in FAA (formalin–acetic acid–alcohol) and preserved in 70 % ethanol upon sampling or after mechanical testing. The middle of peduncles was sectioned in transverse and longitudinal directions either manually using razor blades or mechanically applying a microtome (Vibratome, Hyrax V50; Carl Zeiss MicroImaging GmbH, Jena, Germany) equipped with a sapphire knife. Sections (20–60 μm thick) were stained with Mirande's reagent including green iodine and carmine alumn (Mondolot *et al.*, 2001) or with a solution including acridine red, acriflavin and astra blue (Wacker, 2006). Details of lignification of cell walls were studied by staining with phloroglucinol and hydrochloric acid. Cell-wall and tissue area fractions were quantified by grey-level analyses of cross-sections

TABLE 1. *Fruit weight, peduncle dimensions and characterization of anatomical features of the sclerenchyma in peduncles of mature fruit of 12* Malus *species and one cultivar*

					Peduncle characteristics				
							Sclerenchyma		
No.	Section/series	Species, cultivar	Acc. no (MAL)	Fruit weight (g; mean ± s.d.; $n = 30$)	Length (mm; mean ± s.d.; $n = 30$)	Diameter (mm; mean ± s.d.; $n = 30$)	fb ($n = 10$)	scl ($n = 10$)	ct
1	*Malus/Malus*	*Malus* × *domestica* (Borkh.) 'Pinova'*		190·0 ± 29·12 a	38·9 ± 3·54 a	2·1 ± 0·19 a	Open ring	Thick-walled, open ring/dispersed	1
2		*sylvestris* (L.) Mill.*	0900, 0906	23·8 ± 5·21 bd	24·5 ± 2·76 ef	1·5 ± 0·12 abc	Open ring	Thick-walled, closed ring	1
3		*sieversii* (Ledeb.) Roem. *subsp. Kirghisorum**	0947	28·6 ± 5·11 bc	28·6 ± 4·02 bde	1·3 ± 0·08 bcd	Open ring	Thick-walled, closed ring	1
4		*orientalis* Uglitzk.	0940	20·8 ± 2·90 bd	25·8 ± 5·23 cde	1·2 ± 0·08 cde	Open ring	Thick-walled, closed ring	1
5	*Malus/Baccatae*	*baccata* (L.) Borkh.*	0055, 0467	1·6 ± 0·6 ef	25·3 ± 1·81 def	0·8 ± 0·10 efg	Closed ring	Thin-walled, closed ring	2
6		*hupehensis* (Pamp.) Rhed.	0236	1·5 ± 0·32 ef	45·3 ± 6·09 a	1·0 ± 0·06 def	Open ring	Thin-walled, closed ring	2
7	*Sorbomalus/ Kansuenses*	*fusca* (Raf.) C.K. Schneid.*	0289, 0357	0·4 ± 0·10 f	31·3 ± 3·09 bc	0·7 ± 0·04 gf	Closed ring	Thin-walled, closed ring	2
8		*toringoides* W.E. Hughes	0342, 0735	0·7 ± 0·33 f	27·1 ± 2·19 cde	0·6 ± 0·07 gf	Closed ring	Thin-walled, closed ring	2
9	*Sorbomalus/ Sieboldianae*	*sieboldii* Rehd.	0353, 0747	0·6 ± 0·12 f	31·5 ± 4·21 b	0·6 ± 0·06 g	Closed ring	Thin-walled, closed ring	2
10	*Eriolobus*	*trilobata* (Labill.) C.K. Schneid.	0463, 0566	4·5 ± 1·03 de	33·8 ± 4·22 ab	1·2 ± 0·09 bd	Closed ring	Thin-walled, closed ring	2
11	*Docyniopsis*	*tschonoskii* (Maxim.) C.K. Schneid.	0240	7·9 ± 1·70 cde	18·7 ± 2·74 f	1·7 ± 0·35 ab	Open ring	Thick-walled, closed ring	1
12	*Chloromeles*	*coronaria* (L.) Mill.*	0348, 0723	46·7 ± 7·52 ab	30·5 ± 6·29 bcd	1·4 ± 0·12 bc	Open ring	Thick-walled, open ring/dispersed	1
13		*ioensis* (Wood) Britt.	0134, 0343	64·1 ± 16·13 ab	29·1 ± 4·08 bcd	1·6 ± 0·22 ab	Open ring	Thick-walled, open ring/dispersed	1

Acc. no, accession number; *n*, sample size. Taxonomic affiliation was chosen according to Phipps *et al.* (1990). Based on the occurrence and the arrangement of fibres (fb) and sclereids (scl) in transverse sections, two types of peduncle construction (ct) were distinguished. Species indicated by an asterisk were additionally used for biomechanical tests. Values in a column with the same letter are not statistically different (Kruskal–Wallis one-way ANOVA on ranks followed by an all-pairwise multiple comparison procedure Dunn's method, $P < 0{\cdot}05$; for fruit weight: $H_{12,388} = 378{\cdot}2$, $P \leq 0{\cdot}001$; for peduncle length: $H_{12,388} = 267{\cdot}2$, $P \leq 0{\cdot}001$; for peduncle diameter: $H_{12,388} = 348{\cdot}1$, $P \leq 0{\cdot}001$).

(Image-Pro Plus 7·0; Media Cybernetics, Inc., Bethesda, MD, USA). The mean cell-wall thickness for individual tissues was obtained from the measured values of at least 30 cells. Moreover, the cross-sectional area fraction (total cell area) of individual tissues related to the entire cross-sectional area of peduncle and the cell-wall area fraction of each tissue (only the cell-wall area) related to a defined reference surface (including at least 30 cells) were calculated. During fruit development measurements were carried out with six samples per species and developmental stage, respectively.

Static mechanical tests

Static tension and bending properties of peduncles were determined using a Zwick/Roell BZ 2·5/TS1S universal testing machine (Zwick/Roell, Ulm, Germany). In tensile tests the central 10 mm of 20 peduncles for each accession and each developmental stage was clamped using screw grips, pre-loaded with 0·1 N and pulled with a speed of 1 mm s^{-1}. Force and elongation were recorded during the experiment. By applying Hooke's law assuming conditions of linear elastic behaviour and small deformations the modulus of elasticity E and axial rigidity EA are given as

$$E = \frac{FL_0}{Aw} \text{ and } EA = \frac{FL_0}{w} \tag{1}$$

where F is the applied axial force, w the longitudinal displacement, A the cross-sectional area and L_0 the peduncle test length (Ennos, 2012). The maximum tensile strength σ_{max} at failure was calculated from the formula

$$\sigma_{max} = \frac{F_{max}}{A} \tag{2}$$

In three-point-bending tests the specimens were bent 2 mm at a speed of 5 mm s^{-1} using a bending punch (radius 5 mm). The distance between the supports was adjusted to a span-to-diameter ratio not less than 15, minimizing the influence of shear (Kühlhorn and Silber, 2000). Just before each measurement peduncles were carefully removed from the fruits; fruit weight and peduncle diameter were recorded at three different measuring points. The modulus of elasticity E and flexural rigidity EI were calculated according to

$$E = \frac{1}{48}\frac{FL^3}{Iw_f} \text{ and } EI = \frac{1}{48}\frac{FL^3}{w_f} \tag{3}$$

where F is the applied force, w_f the corresponding deflection, L the distance between the supports and I the second moment of inertia of the sample, which for circular beams of radius r is given by the equation

$$I = \frac{\pi}{4} r^4 \tag{4}$$

To determine mechanical properties of separate tissues a simple micromechanical model was applied assuming that peduncles represent multi-layered composite girders. The Voigt model describes such material of parallel-arranged layers in a parallel circuit of single rigidities, which are weighted by a factor of sample geometry (Niklas, 1992). Assuming that strains in all adjacent, parallel disposed layers (j) have an equal direction and magnitude the effective overall axial rigidity EA or flexural rigidity EI is the sum of all single rigidities (Altenbach *et al.*, 1996) and given by the equations

$$EI = \sum_{j=1}^{n} E_j I_j \text{ and } EA = \sum_{j=1}^{n} E_j A_j \tag{5}$$

Separate tissue layers were carefully removed under a stereomicroscope by scraping with a scalpel, the results were checked after staining with an astrablue–safranin solution and sample geometry was measured. Samples (20 matured peduncles of *M. sylvestris*) were successively bent in three-point bending tests with a small deflection of 1 mm within the elastic range before and after preparation, while for each tensile test freshly prepared samples were stretched until failure. The flexural and axial rigidity of the removed layers result from the difference between rigidities before and after tissue isolation according to eqns (5). Peduncles were kept in water during preparation and between each measurement.

Dynamic mechanical tests

The dynamic mechanical test method (DMA Q800; TA Instruments, New Castle, DE, USA) was applied to characterize the mechanical material behaviour of peduncles under dynamic oscillation conditions in uniaxial tensile tests. Samples were loaded with a sinusoidal dynamic elongation in a displacement-controlled process, given by the equation

$$\varepsilon(t) = \frac{w_0 + \Delta w \sin(2\pi f t)}{L_0} = \varepsilon_0 + \Delta\varepsilon \sin(2\pi f t) \tag{6}$$

where w_0 represents the pre-deformation, Δw the dynamic longitudinal displacement, ε_0 the pre-strain, $\Delta\varepsilon$ the strain amplitude of the specimen and L_0 the length of the pre-deformed sample. The induced harmonic dynamic force answer function and the stimulation oscillate with the same frequency f, but show a phase shift δ (phase angle) between both sine waves.

In viscoelastic materials the phase shift varies between 0° and 90°. The resulting dynamic stress response of the sample with a transverse sectional area A_0 also describes, to a good approximation, a harmonic function (Lion and Kardelky, 2004) of the form

$$\sigma(t) = \frac{F(t)}{A_0} = \sigma_0 + \Delta\sigma\left[\cos(\delta)\sin(2\pi f t) + \sin(\delta)\cos(2\pi f t)\right] \tag{7}$$

The ratio of $\sigma(t)$ and $\varepsilon(t)$ defines the magnitude of the tensile complex modulus E^* composed of a real component and imaginary (i) component in the form of

$$E^* = E' + iE'' \tag{8}$$

The storage modulus E' is defined by the expression

$$E'(f, \Delta\varepsilon, \varepsilon_0) = \frac{\Delta\sigma}{\Delta\varepsilon}\cos(\delta), \tag{9}$$

and the loss modulus E'' by

$$E''(f, \Delta\varepsilon, \varepsilon_0) = \frac{\Delta\sigma}{\Delta\varepsilon}\sin(\delta) \tag{10}$$

To provide information on the relationship between the elastic and inelastic properties in peduncles, the tangent of the phase difference (δ) was calculated according to

$$\tan(\delta) = \frac{E''}{E'} \tag{11}$$

All values of elastic modulus in dynamic mechanical tests are strongly dependent on frequency, strain amplitude, static force and temperature. The setup consisted of a multi-stress mode with a strain sweep from 0·01 to 3 % at a constant frequency of 1 Hz and a multi-frequency mode with a frequency sweep from 0·5 to 6 Hz at constant oscillation strain amplitude of 0·5 %. To prevent buckling a pre-load force of 0·02 N was chosen. In all experiments a peduncle length of 10 mm between the fixed and moveable clamp and a room temperature of 21 °C were retained.

Raman spectroscopic analyses

Two peduncle segments each of six species embedded in hydroxymethylmethacrylate (Technovit 7100; Heraeus Holding GmbH, Hanau, Germany) were analysed by a SENTERRA Dispersive Raman Microscope (Bruker Optik GmbH, Ettlingen, Germany) equipped with a near-infrared laser having a wavelength of 785 nm and laser power of 100 mW. The samples were cut transversely using a rotation microtome (Reichert & Jung, Heidelberg, Germany). Single cell walls were measured at four measuring points per sample including cell walls from 2–4 cells at four positions (90, 180, 270 and 360°) for 8 s. Furthermore, the measuring area across a half transverse section was analysed. The plant-specific lignin was quantified based on wet chemical analyses according to the Klason method (Fengel and Wegener, 1989). For calibration, milled material of *Malus* peduncles and its physical mixtures with microcrystalline cellulose (MCCs) Avicel PH 101 (Sigma Aldrich Chemie GmbH, Munich, Germany) were measured by triple determinations using a MultiRAM FT Raman spectrometer (laser power of 125 mW, spectral resolution of 4 cm^{-1}; Bruker Optik). Peak areas for both the lignin marker band from 1678 to 1561 cm^{-1} ($A_{1678-1561}$) and the polysaccharide marker band from 1171 to 1106 cm^{-1} ($A_{1171-1106}$). Both Raman peak area ratios of the Multiram and Senterra system showed a strong correlation in the lignin content obtained by spectroscopic analyses and wet chemical analyses. Assuming that (1) the lignin and polysaccharide fractions amount to the overall peduncle mass and (2) the proportions between the integrated peak areas and their corresponding masses for the lignin and polysaccharide fraction are constant the following adapted quantity equation for the plant-specific lignin content, w_{lignin} (%), from Raman spectra was used:

$$w_{lignin} = \frac{1}{3{\cdot}903} \times \frac{A_{1678-1561}}{(A_{1678-1561} + A_{1171-1106})} \tag{12}$$

Cellulose I crystallinity was determined by Raman spectroscopic analysis according to Agarwal *et al.* (2010). This method was modified by using the Raman band intensity ratio of the 380 cm^{-1} and polysaccharide marker band due to the higher independence of cellulose microfibril orientation compared with the ratio 380/1096 cm^{-1} (Gierlinger *et al.*, 2010). For a reference system, various MCCs, Avicel RC 581 and PH 101 (Sigma Aldrich Chemie) as well as bacterial cellulose and bleached eucalyptus pulp were predefined ground and analysed by ^{13}C solid nuclear magnetic resonance (NMR) measurements (Newman and Hemmingson, 1994) using a Bruker AVANCE 400 WB spectrometer at 100·13 MHz with CP/MAS and ZrO_2 rotors of 4 mm diameter at 10 kHz spinning speed. The calibration model showed a strong linear relationship between various values of the cellulose crystallinity index X_c as determined by Raman and ^{13}C solid NMR measurements. The adapted quantity equation used for the medium cellulose crystallinity index X_c (%) is given by

$$X_c = \frac{1}{0{\cdot}6298} \times \left(\frac{A_{380}}{A_{1171-1106}} + 0{\cdot}0113\right) \tag{13}$$

Each spectrum was standardized on the embedding system by subtraction of the Technovit-specific band at 603 cm^{-1}.

Data analyses

Non-linear fitting by the Levenberg–Marquardt algorithm served to denote trend lines to measuring points (OriginPro 8·0; OriginLab Corp., Northampton, MA, USA). A *t*-test and one-way ANOVA followed by an all-pairwise multiple comparison procedure was applied to find significant differences between the measured data (SigmaPlot 12; Systat Software, Inc., Richmond, USA).

RESULTS

Anatomy of mature Malus *fruit peduncles*

The fruit weight, peduncle dimensions and anatomical features of the sclerenchymatic tissues of one cultivar and 12 wild species, representatively chosen from all sections of the genus *Malus*, are presented in Table 1. Transverse sections of mature fruit peduncles of all species and the cultivar revealed a central pith parenchyma with slightly thickened and partly lignified cell walls (Fig. 1B, G). Vascular bundles were circularly arranged around the pith with a thin vascular cambium between the xylem and phloem. Generally, the phloem's transverse area fraction (8–12 %) considerably exceeded that of the xylem (3–6 %), while the xylem's area fraction in peduncles of the cultivar *M.* × *domestica* 'Pinova' was highest (Fig. 2). The phloem was enclosed by fibre caps, followed by a layer of sclereids and a cortex composed of isodiametric (polyhedral) parenchyma cells. The cortical parenchyma was

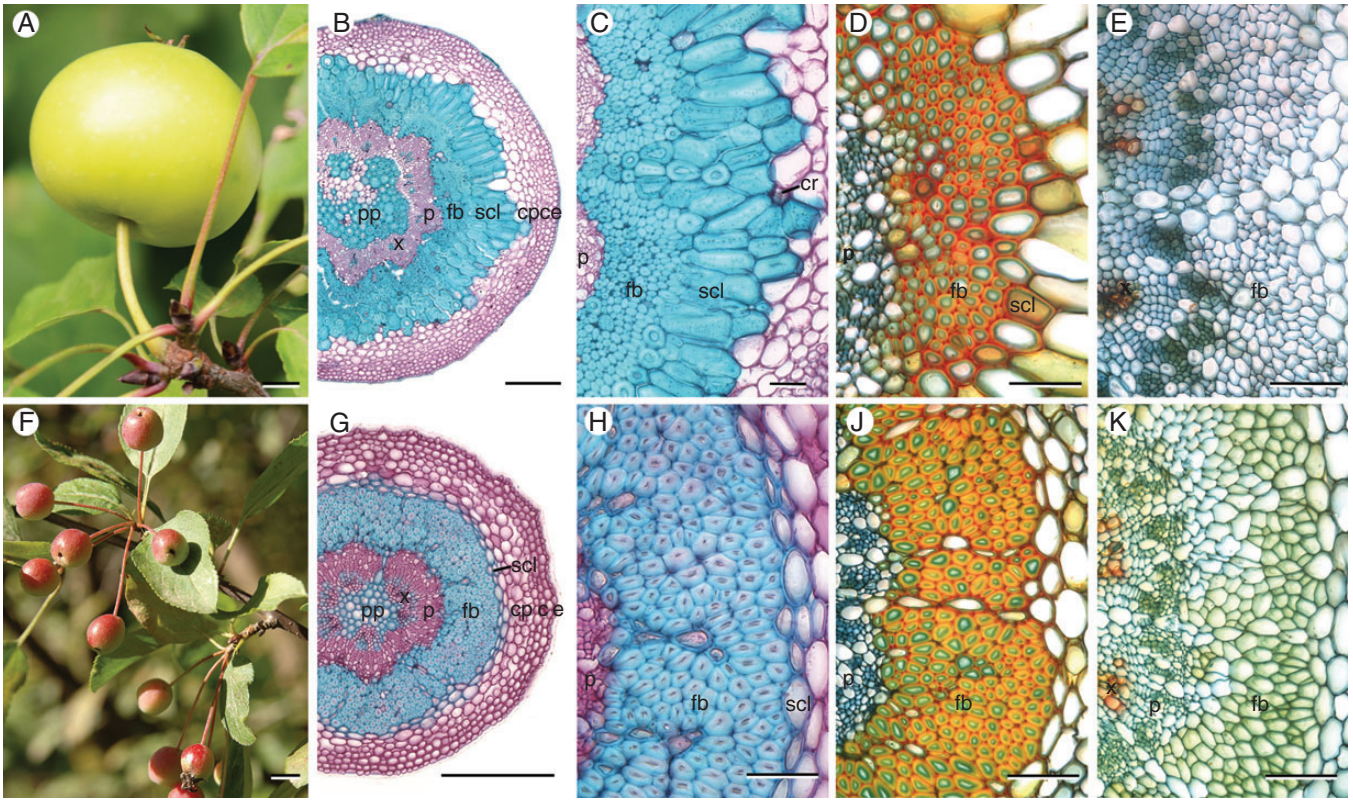

FIG. 1. Fruits and transverse sections of peduncles of *M. sylvestris* (construction type 1, A–E) and *M. fusca* (type 2, F–K) at different stages of fruit development. (B, C) Fibre caps in matured peduncles of type 1 are arranged in an open, flower-shaped ring – enclosed by a massive ring of thick-walled sclereids. (G, H) Mature peduncles of type 2 possess a closed ring of fibres – enclosed by a small layer of thin-walled sclereids. (D, J) Fibres with moderately thickened, lignified cell walls (primary cell-wall layers in green), and beginning formation of sclereids 18 d after full bloom. (E, K) In pedicels only scattered vessels are lignified. Staining: (B, C, G, H) Carmino Verte de Mirande; lignified tissues are stained green-blue, cellulose cell walls pink. (B, C, G, H) Wacker; lignified tissues are stained red–orange, cellulose cell walls green–blue. Scale bars: (A, F) = 10 mm; (B, G) = 200 μm; (C–E, H–K) = 50 μm. Abbreviations: c, collenchyma; cp, cortical parenchyma; cr, crystal clusters; e, epidermis; fb, fibres; p, phloem; pp, pith parenchyma; scl, sclereids; x, xylem.

always the dominant tissue (Fig. 2). A lamellar collenchyma (two to four cell rows) and an epidermis, covered with a partly thick cuticle (e.g. *M. fusca*), surrounded the cortex. Often the initial development of periderm was observed in peduncles of mature fruits. Due to anatomical differences in the arrangement of sclerenchyma between the different species two types of construction could be distinguished (Table 1). In type 1 the fibre caps were arranged in an open, flower-shaped ring followed by thick-walled brachysclereids (Fig. 1B, C). This type was mainly found in peduncles of accessions of the series *Malus* and the North American section *Chloromeles*. Average peduncle diameters exceeded 1·2 mm, and supported apple fruits weighing more than 8 g (Table 1). Sclereids either formed a voluminous, closed ring around fibre caps (e.g. in *M. sylvestris*), or were arranged in an open ring. Additionally, they could be dispersed within the cortical parenchyma (e.g. in the cultivar 'Pinova'). Clusters of calcium oxalate druses were frequently found in parenchyma cells near sclereids (Fig. 1C). Type 2 was found in accessions within the series *Baccata* and sections *Sorbomalus* and *Eriolobus* with small fruits hanging in clusters. Directly adjacent to the fibres, these peduncles possessed one or two rows of parenchyma cells with only slightly thickened, lignified cell walls (Fig. 1G, H). Thus, the maximal cell-wall area fraction of this tissue reached 28 %, regarded as relative tissue density (Fig. 3H). These cells were not sclereids in the general sense of the term referring to lignified, thick-walled, dead cells. However, other authors use the term more widely (Heide-Jorgensen, 1990; Evert, 2006). In the following these cells are called 'thin-walled sclereids', because distinguishing them from sclerified parenchyma was difficult. Only cells that possessed thick secondary cell walls, numerous ramified pits and cell-wall area fractions of about 90 % were defined as 'thick-walled sclereids' (Figs 1C and 3D). Nonetheless, transitional forms were also observed.

Fruit development-related peduncle anatomy and biomechanics

The consecutively, anatomical and biomechanical tests included peduncles of five species and one cultivar represented each construction type according to Table 1 (asterisks). The modulus of elasticity of peduncles of the European crab apple (*M. sylvestris*) belonging to type 1 increased gradually with increasing fruit weight (Fig. 3A, B). In that case the modulus of elasticity characterized the stiffness of a complex, heterogeneous structure, called structural modulus (Niklas, 1992). The structural modulus for pedicels at flowering time ranged from 0·08 to 0·14 GPa. Supporting tissues were restricted to the first lignified vessels (area fraction of 1·2 %) and subepidermal lamellar collenchyma (area fraction of 19 %) (Fig. 3D). Fibre caps with

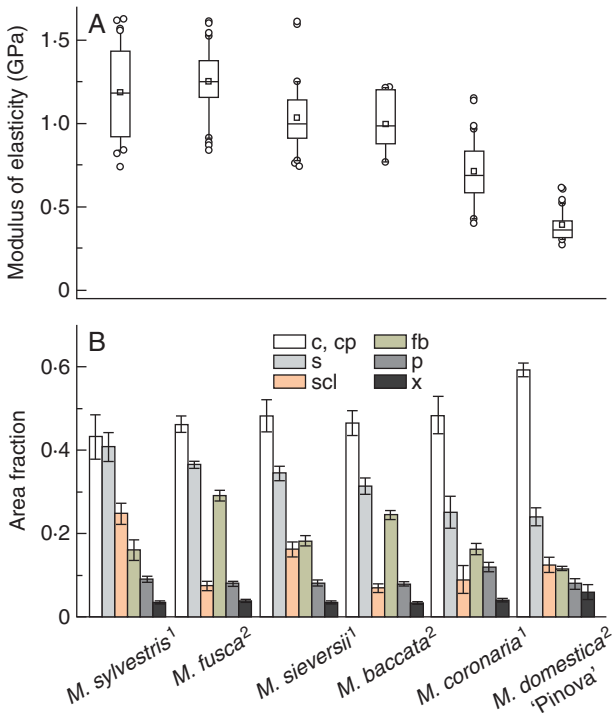

FIG. 2. (A) Structural modulus of elasticity obtained from static three-point bending tests of matured peduncles of different *Malus* accessions and types of construction according to Table 1 (index) ordered by magnitude. Central boxes represent the 25th and 75th percentiles with the median (line) and mean (square). Whiskers indicate the 10th and 90th percentile, and outliers are shown as circles. (B) Cross-sectional area fractions of single tissues of peduncles. High proportions of peripherally arranged cortical parenchyma with the highest contribution to the axial second moment result in decreased structural elastic modulus of the whole peduncle structure. Error bars are standard deviations. Abbreviations: c, collenchyma; cp, cortical parenchyma; fb, fibres; p, phloem; s, sclerenchyma (fibres and sclereids); scl, sclereids; x, xylem; 1, type 1; 2, type 2.

thin primary cell walls ($0{\cdot}5 \pm 0{\cdot}1$ μm) were recognizable (Fig. 1E). The cross-sectional area of peduncles increased during fruit development by about 1·1 mm^2 (60 %) until day 60 of the monitoring period. Due to cambial growth mainly phloem cells were formed, while the remaining increase in diameter was based on cell elongation and division of cortical parenchyma cells. Fibres reached their final dimensions with a length of about $430{\cdot}3 \pm 10{\cdot}5$ μm, diameter of $13{\cdot}4 \pm 2{\cdot}9$ μm and cell-wall thickness of $7{\cdot}1 \pm 1{\cdot}4$ μm, resulting in cell-wall area proportions of 96 % at about day 37 after full bloom. Originating from cortical parenchyma and starting in cells which are directly adjacent to fibres, a large ring of sclereids differentiated time-delayed (Fig. 1D). This can also be seen from decreasing cross-sectional area fractions of parenchyma (Fig. 3D). At about day 37 sclereids represented a cross-sectional area fraction of 25 %. Until this stage the modulus of elasticity increased considerably by 0·71–0·84 GPa, the maximum tensile strength by 11·5 MPa and the breaking force by 19·8 N (Fig. 3B, C). However, during subsequent fruit development the maximum tensile strength of peduncles remained constant. The breaking force increased slightly by 7 N, while the modulus of elasticity of peduncles still increased by an additional 0·33–0·46 GPa, caused by further thickening of sclereid cell walls. Sclereids reached their maximum cell-wall thickness of $13{\cdot}6 \pm 3{\cdot}2$ μm and cell-wall proportions of 89 % only at fruit maturity.

For fruit peduncles of the Oregon crab apple (*M. fusca*) belonging to type 2 the graphs display a different pattern from those of type 1 (Fig. 3E–H). The closed fibre ring reached its maximum cross-sectional area fraction of 30 % with cell-wall proportions of 93 % even by day 37 (Fig. 3H). In one or two cell layers of the parenchyma directly adjacent to fibres, cell walls thickened from about day 18 (Fig. 1J). Thin-walled sclereids comprised small area fractions of just 5–7 % with maximum cell-wall proportions of about 28 % at the mature stage (Fig. 3H). Note that the cross-sectional area proportions of the whole sclerenchyma in *M. fusca* resembled those of *M. sylvestris* (Fig. 2). Altogether, the peduncle cross-sectional area expanded by about 0·08 mm^2 (28 %) until day 18, caused by the formation of vascular tissue and cell elongation of fibres and parenchyma. Cell division of cortical parenchyma was not observed. The development of the whole sclerenchyma corresponded to a marked increase in modulus by 1·0–1·2 GPa. The maximum tensile strength increased by about 38·5 MPa and the breaking force by 13·1 N (Fig. 3E). Until fruit maturity, peduncle strength and stiffness remained constant, because cell walls of fibres were fully developed and walls of sclereids not further thickened.

In comparison with static tensile tests, which primarily describe the elastic behaviour of a material, the moduli determined in dynamic tests provide additional information about viscous properties. The storage modulus E' constitutes the dominant component of the complex modulus E^* in all mechanically tested species. Hence, the complex modulus E^* in peduncles of *M. sylvestris* (type 1) primarily increased due to a noticeable rise of the storage modulus E' by 1·14 GPa (at strain amplitudes of 0·2 %) until fruit maturity (Fig. 4A). E' represents the elastic component, which is proportional to the stored energy in a system during one load cycle. However, the loss modulus E'' indicates the viscous material properties and is related to the energy dissipation in a material. It slightly increased by 0·14 GPa (at strain amplitudes of 0·2 %) until day 60 and remained constant thereafter, while the values of E' continuously increased by a further 0·63–0·81 GPa. An increasing dependence of E'' on the deformation amplitude was clearly evident from day 18, whereas E'' of pedicels was virtually independent of the current deformation (Fig. 4C). Deformation amplitudes above 0·5–0·7 % resulted in decreased loss modulus. The storage modulus decreased immediately with increasing deformation amplitudes. The tangent of the phase difference between E' and E'', the loss factor, is regarded as a damping parameter and provided information on the relationship between the elastic and inelastic material properties in a material. High loss factors indicate a higher energy dissipation of a material caused by energy transformation. For all *Malus* accessions, values increased with stronger deformation amplitudes ranging from 0·15 to 0·32. In peduncles of type 1 (e.g. *M. sylvestris*), loss factors were constant or increased slightly until day 60 (Fig. 4B). Subsequently, values of tanδ decreased, whereas damping remained constant in peduncles of type 2. While all dynamical moduli increased with higher frequencies of the dynamic oscillation load, the damping decreased because inelastic deformations were less affected (data not shown).

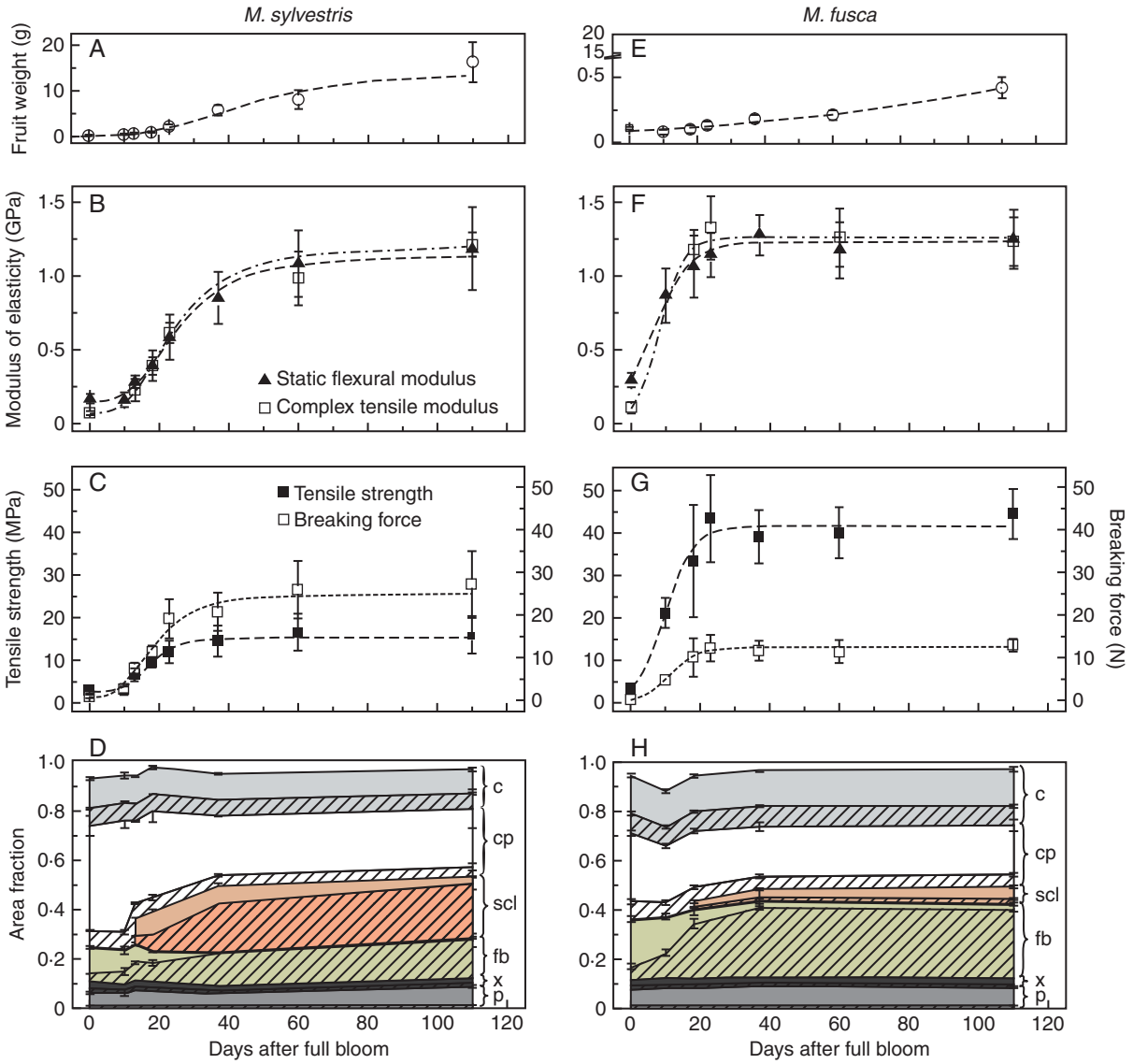

FIG. 3. Comparison of peduncles of *M. sylvestris* (type 1, A–D) and *M. fusca* (type 2, E–H) during one growing season. Fruit weight, structural modulus of elasticity, maximum tensile strength and breaking force as well as cross-sectional area fractions of single tissues with their cell-wall area proportions are shown. The structural modulus of elasticity was calculated by applying strains of 0·05–0·25 % in static tests or 0·2 % in dynamic tests. Error bars are standard deviations; lines indicate the trends, based on non-linear fitting. The cross-sectional area fractions of single tissues are shown as different colours and their cell-wall area proportions are hatched. Abbreviations: c, collenchyma; cp, cortical parenchyma; e, epidermis; fb, fibres; p, phloem; scl, sclereids; x, xylem.

Biomechanics of peduncles with isolated tissues

Peduncles of *M. sylvestris* at three conditions were successively subjected to mechanical tests: (I) complete peduncles; (II) peduncles after careful removal of layer 1 comprising the epidermis, collenchyma and cortical parenchyma; and (III) peduncles after removal of layer 1 and layer 2 containing sclereids. The measured and then calculated mechanical parameters of the removed peduncle layers (asterisks) are presented in Fig. 5. The outer layer 1 of peduncles exhibited the significant smallest structural modulus of elasticity, with a median of 0·15 GPa (Fig. 5A). Consequently, layer 1 contributes 12 or 4 % of the overall flexural or axial rigidity, respectively (Fig. 5B). The highest modulus with a median of 3·62 GPa was measured for the inner layer 3, containing fibres, phloem, xylem and pith. For the layer of thick-walled sclereids (layer 2) an elastic modulus of 2·16 GPa was calculated. Layer 3 accounts for about 61 % to the overall axial rigidity under tensile loads and the layer of sclereids about 35 %. Sclereids contributed about 58 % to the overall flexural rigidity in bending, while the inner layer 3 contributed about 30 %. The breaking force under tensile load remained nearly constant, reaching a median of 30 N (Fig. 5C). For layer 3 only slightly smaller breaking forces were measured after isolation of the outer layers. Because of the approximately constant breaking force and decreasing transverse sectional areas owing to tissue removal, the calculated tensile strength increased (Fig. 5C).

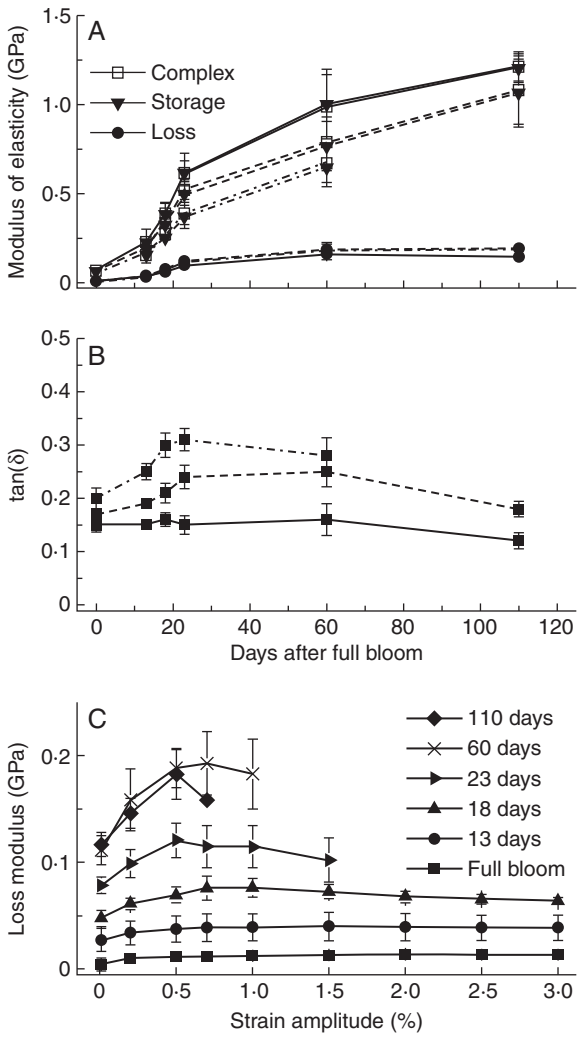

FIG. 4. (A) Complex, storage and loss modulus, and (B) the loss factor of peduncles of *M. sylvestris* (type 1) during one growing season measured in dynamic tensile tests. Solid lines denote the values at strain amplitudes of 0·2 %, broken lines at 0·5 % and dashed/dotted lines at 1·0 %. (C) The loss modulus dependent on the strain amplitude and development stage (at a constant frequency of 1 Hz).

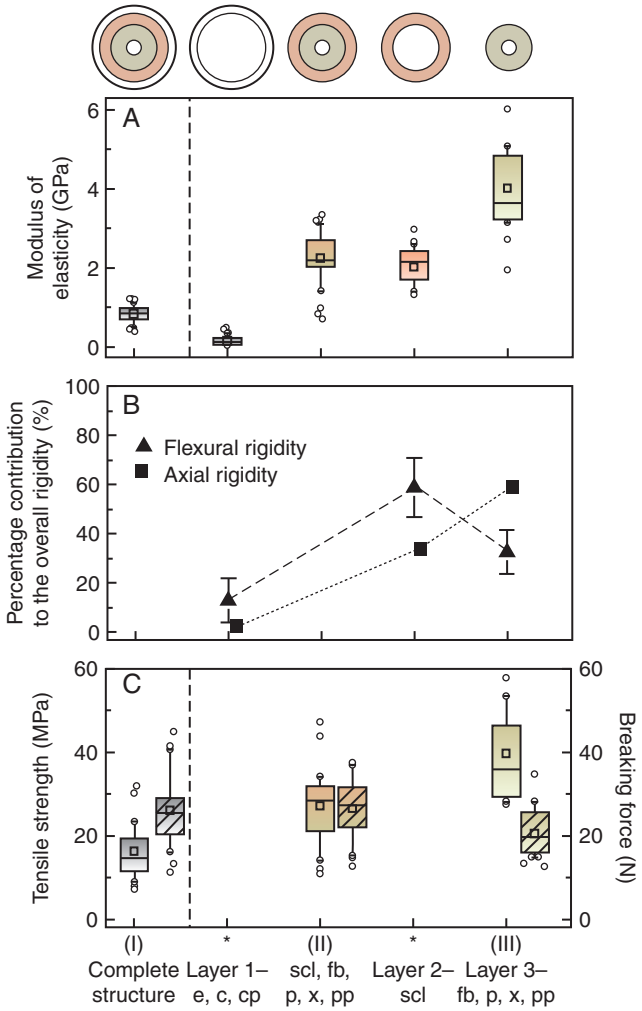

FIG. 5. (A) Measured (I–III) and calculated (asterisks) modulus of elasticity, (B) proportional contribution of individual layers to overall flexural and axial rigidity (mean with SD) and (C) maximum tensile strength and breaking force (hatched) of the whole structure and single tissue layers of peduncles of *M. sylvestris* (type 1, from left to right). Central boxes represent the 25th and 75th percentiles with the median (line) and mean (squares). Whiskers indicate the 10th and 90th percentiles, and outliers are shown as circles. Abbreviations: c, collenchyma; cp, cortical parenchyma; e, epidermis; fb, fibres; p, phloem; pp, pith parenchyma; scl, sclereids; x, xylem.

Raman spectroscopy

Raman spectroscopy served to evaluate the topochemical distribution of secondary cell-wall components in fibres and sclereids for improved understanding of the previously determined mechanical properties. Investigations of cell walls of single fibres and sclereids in type 1 peduncles revealed a median lignin content of 17·7–19·6 %. Thick-walled sclereids of *M. sieversii* and the cultivar 'Pinova' possessed a slightly higher lignin content compared with fibres (not statistically significant, test statistics in Table 2), while in accessions of *M. sylvestris* and *M. coronaria* both tissues showed similar values as seen in Raman spectra for a transverse section of *M. sylvestris* (Fig. 6D). For the wave number range of 1678–1561 cm^{-1}, characteristic for –C = C– bonds in the aromatic compounds of lignin, the highest intensity was found at positions of sclereids and fibres. The corresponding lignin content, calculated from five series of a transverse measuring field, revealed similar mean values of 19·2 % for both sclereids and fibres (Fig. 6A). However, secondary cell walls of the latter in type 2 peduncles (*M. baccata* and *M. fusca*) had a significantly lower lignin content (medians of 10·8–13·6 %) compared with those in type 1 (test statistics in Table 2). Due to weak Raman spectra, values for thin-walled sclereids in peduncles of type 2 were difficult to evaluate.

The cellulose crystallinity index describes the relative amount of crystalline (ordered) regions of cellulose, which has considerable influence on stiffness and strength of secondary cell walls. It differed significantly between fibres in peduncles of type 1 and type 2 and between fibres and thick-walled sclereids in all investigated peduncles of type 1 (test statistics in Table 2). Cellulose fibrils in individual fibres showed a higher degree of orientation compared with that sclereids. The cellulose crystallinity index I_{cr}

TABLE 2. *Comparison of lignin content and cellulose crystallinity index of fibres and sclereids of different* Malus *accessions determined by Raman spectroscopic analyses in transverse sections of matured peduncles*

Species, cultivar	*n*	Lignin content (%)			Cellulose crystallinity index (%)		
		Fibres (mean ± s.d.)	Sclereids (mean ± s.d.)	Test statistics	Fibres (mean ± s.d.)	Sclereids (mean ± s.d.)	Test statistics
				Construction type 1:			
M. sylvestris	16	19·5 ± 1·1 a	19·1 ± 0·7 ab	$P = 0{\cdot}252$, $t = 1{\cdot}2$	80·2 ± 6·8 a	59·5 ± 10·9 a	$P < 0{\cdot}001$, $t = 5{\cdot}9$
M. sieversii ssp. *Kirghisorum*	32	18·7 ± 1·3 a	19·5 ± 1·0 a	$P = 0{\cdot}008$, $t = -2{\cdot}8$	68·9 ± 13·9 ab	48·4 ± 10·4 b	$P < 0{\cdot}001$, $t = 6{\cdot}8$
M. × *domestica* 'Pinova'	16	17·8 ± 1·1 ab	18·8 ± 0·8 ab	$P = 0{\cdot}009$, $t = -2{\cdot}8$	56·8 ± 9·9 bc	42·3 ± 5·0 b	$P < 0{\cdot}001$, $t = 282{\cdot}0$
M. coronaria	32	18·0 ± 1·8 a	18·7 ± 1·6 b	$P = 0{\cdot}147$, $t = -1{\cdot}5$	73·8 ± 13·2 ab	60·6 ± 14·6 a	$P = 0{\cdot}005$, $t = 638{\cdot}0$
				Construction type 2:			
M. baccata	32	11·1 ± 1·9 c			36·6 ± 3·7 d		
M. fusca	32	14·1 ± 2·1 bc			48·5 ± 12·1 c		

n, sample size. Data are from four measurements (at 2–4 single cells) at four different regions in transverse sections of two peduncles of each species, respectively; only one sample for both *M. sylvestris* and the cultivar 'Pinova'. Test statistics: *t*-test, Mann–Whitney rank sum test, *P* values indicating statistical differences between values of fibres and sclereids. Values in a column with the same letter are not statistically different (for the lignin content of sclereids: one-way ANOVA $F_{3,94} = 3{\cdot}3$, $P = 0{\cdot}025$ followed by an all-pairwise multiple comparison procedure Tukey test, $P < 0{\cdot}05$; other parameters Kruskal–Wallis one-way ANOVA on ranks followed by an all-pairwise multiple comparison procedure Dunn's method, $P < 0{\cdot}05$; for the lignin content of fibres: $H_{5,155} = 109{\cdot}9$, $P \leq 0{\cdot}001$; for the cellulose crystallinity index of fibres: $H_{5,143} = 95{\cdot}2$, $P \leq 0{\cdot}001$; for the cellulose crystallinity index of sclereids: $H_{3,94} = 33{\cdot}3$, $P \leq 0{\cdot}001$).

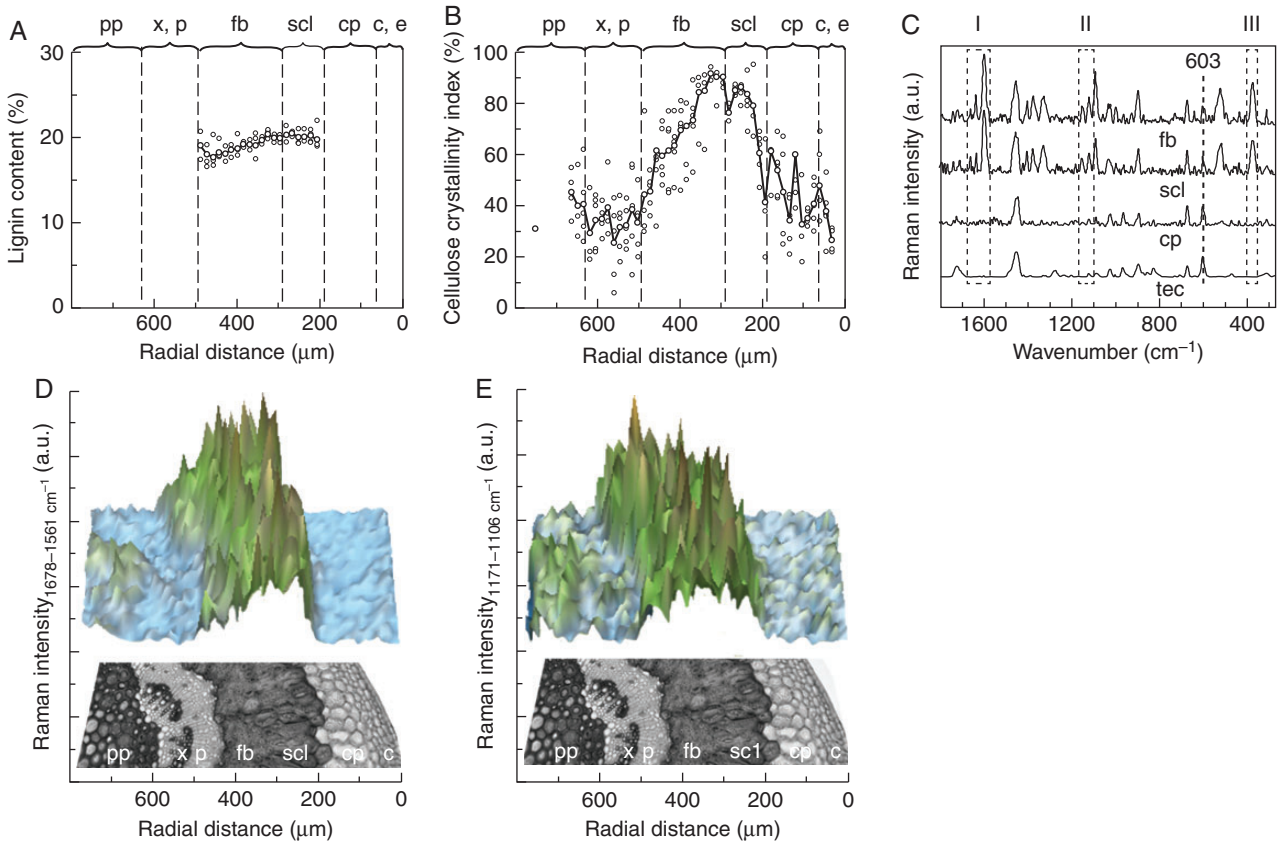

FIG. 6. (A) Distribution of lignin content and (B) the cellulose crystallinity index across a peduncle transverse section of *M. sylvestris*. (C) Representative Raman spectra of the embedding polymer Technovit and the peduncle tissues cortical parenchyma, sclereids and fibres normalized using the Technovit-specific peak at 603 cm^{-1} with marker bands for lignin (I), polysaccharides (II) and the cellulose crystallinity index (III). (D) Raman intensities calculated by integrating over defined wave number areas from 1678 to 1561 cm^{-1} for lignin and (E) from 1171 to 1106 cm^{-1} for polysaccharides. Abbreviations: c, collenchyma; cp, cortical parenchyma; e, epidermis; fb, fibres; p, phloem; pp, pith parenchyma; scl, thick-walled sclereids; tec, Technovit; x, xylem.

across a transverse section of *M. sylvestris* rose from about 20–50 % in phloem and pith to about 90 % in fibres and decreased again in the cortical parenchyma (Fig. 6B). Based on skeletal vibrations occurring in the spectral range between 1165 and 1065 cm^{-1}, the highest Raman intensity of the polysaccharide fraction across the transverse section was found in fibres and sclereids (Fig. 6E). Increased intensities occurred also in the pith parenchyma and lamellar collenchyma, both exhibiting thickened cell walls.

DISCUSSION

Apple fruit peduncles are small structures that constantly adjust their supporting tissues with respect to the steadily increasing fruit weight. At the same time, transport of nutrients must be ensured and detachment of fruits for dispersal by the formation of an abscission zone (Namikawa, 1922; Lang and Ryan, 1994; Sun *et al.*, 2009).

Anatomy

The similar anatomy found in *Malus* peduncles of 12 wild species and one cultivar, including a circular arrangement of epidermis, collenchyma, cortical parenchyma (dominant tissue), centrally sclerenchyma, phloem, xylem and a partly lignified pith parenchyma, corresponds to previous descriptions of different fruit peduncles of Rosaceae (Schwarz, 1929). While the fibre ring is a constant anatomical character of sclerenchyma, we have observed interspecific differences with respect to differentiation of brachysclereids, their proportions and arrangement. Accordingly, two types of peduncle construction have been identified dependent on peduncle diameter and fruit weight: (1) a large, closed or open ring of thick-walled sclereids around fibre caps, and (2) thin-walled sclereids, forming one to two cell rows (Table 1). The xylem is restricted to scattered vessels in all investigated wild accessions, whereas a regular xylem cylinder usually contributing to the flexural rigidity of young branches is only found in peduncles of the cultivar ‘Pinova’. Reaction xylem containing tension wood fibres analogous to infructescences of *Kigelia pinnata* and *Couroupita guianensis* (Sivan *et al.*, 2010) has not been observed.

Mechanical relevance of different tissues

The peripherally arranged lamellar collenchyma represents the main supporting tissue in pedicels (flower stalks), as known from many growing organs or herbaceous plant stems (Evert, 2006; Leroux, 2012). First, the low overall structural elastic modulus of apple pedicels (Fig. 3) corresponds to the value of the peripheral soft layer (epidermis, collenchyma, parenchyma) in peduncles of *M. sylvestris* (Fig. 5). Secondly, it is also in accordance with a structural modulus, which can be calculated from the sum of corresponding single rigidities using known moduli of collenchyma (0·08 GPa) and parenchyma (0·04–1 GPa), respectively (Niklas, 1992; Rüggeberg *et al.*, 2009*a*). Commonly, plastic deformations and the low stiffness of both tissues relate to the structure of primary cell walls, in which cellulose microfibrils are interconnected by hemicelluloses, pectin and glycoproteins (Niklas, 1992; Gibson, 2012; Leroux, 2012). Additionally, the low cellulose crystallinity index in cell walls of collenchyma and cortical parenchyma revealed by Raman spectroscopy in *M. sylvestris* peduncles points to a lower tissue stiffness and strength (Fig. 6B). The values resemble those for bark and phloem in some trees (24–39 %), determined by X-ray diffraction (Parameswaran, 1975). The degree of cross-linking and crystallinity of cellulose I is higher in microfibrils of secondary than of primary cell walls (Haigler and Weimer, 1991). Regulation of the synthesis of cellulose fibrils by the cellulose synthase complex, however, is a dynamic, not yet understood process that can be influenced by external mechanical stresses (Wu *et al.*, 2000; Harris *et al.*, 2009). Nevertheless, the peripherally arranged soft tissue layer significantly influences the flexural rigidity of the peduncle (Fig. 5) due to its strong involvement in the total second moment of inertia (66 %) (Rees, 2009). During tensile loading the contribution of the soft tissue layer (layer 1) to the axial rigidity of the whole structure is one-quarter smaller, despite this tissue layer having large proportions of the cross-sectional area (42 %). A marked contribution to the breaking force of peduncles has been not detected, whereas in herbaceous stems the epidermis plays an important role in absorbing negative tensile stresses and circumferential strains caused by hydrostatically inflated parenchyma cells in the cortex (Niklas and Paolillo, 1998).

The dynamic mechanical tests have experimentally verified that, in particular, the viscous properties of the parenchyma contribute to the ability of peduncles to dissipate energy under oscillating longitudinal loads. The greatest increase in loss modulus is associated with rising amounts of cortical parenchyma due to cell expansion and division. During this phase the viscous damping, referred to as structural damping by Spatz and Theckes (2013), increases, which is more pronounced at higher strains (Fig. 4). Obviously, high longitudinal strain amplitudes are damped more effectively in peduncles with high amounts of parenchyma cells. This possibly explains why peduncles of domesticated apples possess high proportions of cortical parenchyma, resulting in a more flexible structure (Fig. 2). Selective breeding, however, should be taken into account. Parenchyma cells filled with aqueous living protoplasm may be regarded as liquid-filled, pressurized foam (Niklas, 1989; Gibson, 2012). Water is virtually incompressible, resulting in increased dynamic moduli of peduncles at higher frequencies of dynamic oscillation loads. A dissipation of energy is conceivable by friction across cell contact areas or by deformations of the thin elastic cell walls in the direction of intercellular spaces. The latter are filled with air, which are about 20 000 times more compressible than water. An interaction between relative tissue density, turgescence and stiffness of parenchyma is known (Niklas, 1988), and hence an influence on viscous damping can be assumed. Previous studies have (1) revealed compaction behaviours of the thick exo- and mesocarp of pomelo fruits [*Citrus maxima* (Burm.) Merr., Rutaceae] attributed to a gradual change in parenchyma density interspersed by vascular bundles (Thielen *et al.*, 2013), (2) assigned the largest contribution to damping in palms to the parenchymatic core reinforced by numerous vascular bundles due to gradients of stiffness along their fibre caps (Rüggeberg *et al.*, 2009*b*), and (3) identified the hierarchical branching in trees as an important factor for damping, dissipating theoretically up to 30 % of the total energy during one bending oscillation through wind loads (James *et al.*, 2006; Theckes *et al.*, 2011; Spatz and Theckes, 2013).

Peduncle stiffness and especially their elastic component markedly increase after developing secondary cell walls of

fibres and sclereids, as seen under dynamic oscillation conditions in tensile tests (Figs 3 and 4). During this process the inner layer (layer 3) containing prosenchymatic fibres contributes most to overall axial rigidity under tensile stresses and has the highest modulus of elasticity (Fig. 5). This influence is almost twice that of sclereids, although the area fraction of fibres was about 1·5 times smaller. Correspondingly, fibres in peduncles of *M. sylvestris* (type 1) which bear heavier fruits, have a significantly higher lignin content and an about 1·8-fold higher cellulose crystallinity index than those of *M. fusca*, belonging to type 2 (Table 2). Commonly, plants can adapt their cell-wall stiffness by varying levels of lignin content, cellulose microfibril crystallinity and their orientation (Köhler and Spatz, 2002; Goswami *et al.*, 2008; Burgert and Fratzl, 2009). According to calculations in sensitivity analyses by Placet *et al.* (2012), the shear modulus of the amorphous cellulose is the dominant parameter influencing the longitudinal elastic modulus of hemp fibres (*Cannabis* L., Cannabaceae), besides fractions of crystalline cellulose and their longitudinal elastic modulus.

As compared with the inner fibre layer, the layer of thick-walled sclereids (layer 2) of *M. sylvestris* peduncles exhibits on average 1·7 times smaller modulus of elasticity (Fig. 5). This may be due to the lower cellulose crystallinity index of sclereid cell walls, while the lignin content is similar (Table 2). Sclereids on cell cultures of *Pinus radiata* D.Don. (Pinaceae) possessed a higher lignin content compared with tracheary elements, but also variable values within the wall of one individual cell (Möller *et al.*, 2005). The isodiametric cell shape of brachysclereids combined with many intercellular spaces reducing the number of stiff interfaces between individual cells could be another explanation for the lower tissue stiffness and strength. The observed gradual increase of crystallinity index from parenchyma to sclerenchyma in peduncles of *M. sylvestris* may be helpful in gradually reducing stress discontinuities (Fig. 6B; Rüggeberg *et al.*, 2009*b*). Despite their lower elastic modulus the peripheral position of brachysclereids results in a four-fold larger axial second moment of area compared with centrally positioned fibres. Consequently, sclereids contribute about twice as much to the overall flexural rigidity of the structure and are more effective under bending stresses (Fig. 5).

Given the viscous properties of *Malus* peduncles, sclereids can be regarded as regulating elements between structural damping and stiffness. The formation of sclereids from parenchyma cells results in decreased loss factors (Fig. 4B). The increased dependence of the viscous component upon deformation amplitudes during stiffening of parenchyma appears to be similar to the strong non-linear viscoelastic behaviour of filled technical elastomers (Wrana *et al.*, 2003). The highest loss modulus applying deformation amplitudes of 0·7 % denotes the maximum internal structural friction in intact peduncles (Fig. 4C). Larger deformations probably result first in structural damages.

While the stiffening of peduncles under bending and tensile stresses influences both fibres and brachysclereids, an increase in breaking force and maximum tensile strength is mainly attributed to fibres. The removal of brachysclereids resulted in only slightly decreased breaking forces in our investigations of *M. sylvestris* and may be referable to the high cellulose crystallinity index of fibres (Fig. 5). Generally, tensile yield as well as maximum strength are influenced by microstructural characteristics of a material, correlating with the density and elastic modulus of wood (Gibson, 2012). Crystalline domains of cellulose fibrils play an important role. They contribute about 30–40 % to the overall strain of primary phloem fibres of flax (*Linum usitatissimum* L., Linaceae) due to the stretching of crystals, while the remaining strain is caused by the alignment of non-crystalline domains (Kölln, 2004). All tested peduncles fail at forces higher than the maximum fruit weight is exerting. Thus, peduncles are highly reliable even under extreme conditions, providing safety factors ranging from 30 in cultivars to about 2700 in *M. fusca*, a feature already discussed by Schwarz (1929).

The underlying mechanism of tissue adaptation

During secondary growth the vascular cambium generates mainly phloem with high proportions of sieve tubes, ensuring sufficient assimilate flow in peduncles (Lang and Ryan, 1994). Some cultivars attain their xylem's full conducting capacity shortly after the pedicel has reached its final length (Drazeta *et al.*, 2004). In contrast, the growth rate of xylem in most trees is frequently larger than that of phloem (Evert, 2006). The resulting increase in phloem girth entails cell elongations and divisions of cortical parenchyma by pushing outer tissues to the periphery. However, calculations here revealed that the increase in parenchyma mostly exceeds the forced increase in structure girth due to phloem formation. Fibres undergo a coordinated growth, but new fibres cannot be formed. Hence, the fibre ring is relatively displaced to the centre, which would result in a less stiff peduncle especially with respect to bending (Fig. 7). Cortical parenchyma cells outside the fibre ring differentiate into sclereids by reinforcing their cell walls, providing a rigid structure.

The above mechanism of secondary growth has been observed in peduncles of type 1, which support heavier fruits (more than 8 g), resulted in diameters greater than 1·2 mm (Table 1). Only these *Malus* species develop thick-walled sclereids in addition

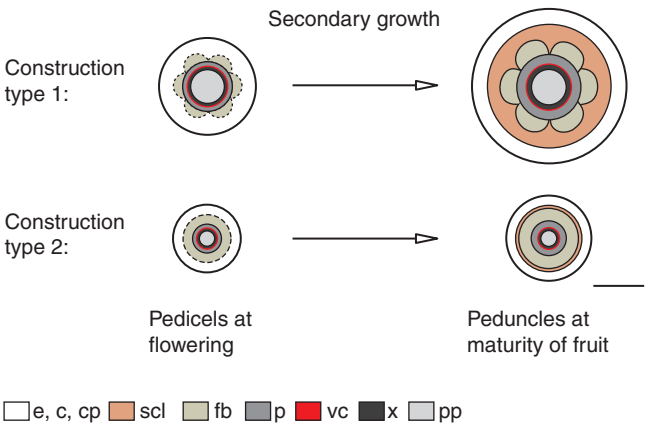

FIG. 7. Schematic representation of the secondary growth of two different types of *Malus* peduncle construction. The increase in peduncle girth of type 1 due to cambial phloem formation entails cell elongations and division of cortical parenchyma by pushing outer tissues to the periphery. The fibre ring is displaced to the centre. The differentiation of cortical parenchyma cells outside the fibre ring into brachysclereids stiffens the structure most effectively against bending. Scale bar = 500 μm. Abbreviations: c, collenchyma; cp, cortical parenchyma; e, epidermis; fb, fibres; p, phloem; pp, pith parenchyma; scl, sclereids; vc, vascular cambium; x, xylem.

to fibres. Peduncles of type 2 bearing small fruits (less than 8 g) produce a slender ring of thin-walled sclereids in addition to fibres, also found in peduncles of different species of the genus *Prunus*.

Prosenchymatic fibres generate peduncle strength and stiffness predominantly in the axial direction. Sclereids act as 'accessory' cells, which enhance the proportion of sclerenchyma, mostly stiffening the structure against bending. In view of our investigations this mechanism can be understood as an adaptation to changing fruit weights. As previously reported, the sclereid density increases to strengthen exposed *Camellia* petals under the influence of external forces by rainfall was interpreted as a function-related process (Zhang *et al.*, 2010). Whether the mechanism is active, e.g. force-triggered, remains open. Previous studies revealed sclereid initials in response to larger nuclei, higher concentrations of plant hormones (IAA) or a strong positional influence of cell differentiation (Boyd *et al.*, 1982; Savidge, 1983; Evert, 2006). The 'filling' of enlarged gaps between fibre caps using sclereids is comparable to liana stems (Busch *et al.*, 2010) and can additionally stabilize peduncles against torsion. Furthermore, a protective effect on essential structures against pests should be considered (Franceschi *et al.*, 2005).

Our experimental data reveal specific mechanical properties of brachysclereids and emphasize their specific role in addition to fibres in *Malus* fruit peduncles related to tissue modification due to increasing fruit weights. These findings confirm previous, mechanically unassigned assumptions that sclereids generally strengthen the plant structure. However, we show that brachysclereids contribute to the stiffness mostly under bending (flexural rigidity) rather than to the strength during tensile loads, and verify their effect on viscous damping.

ACKNOWLEDGEMENTS

W. Marx and K. Götze (Horticultural test field at the Saxon State Office for Environment, Agriculture and Geology, Dresden-Pillnitz, Germany) are acknowledged for permission to take samples. We thank A. Winkler and P. Stelling (Institute of Lightweight Engineering and Polymer Technology, ILK, Technical University Dresden, Germany) for their support in using DMA, as well as D. Voigt (Institute of Botany, Technical University Dresden, Germany) and two anonymous reviewers for suggestions that helped to improve the manuscript. This research was funded by the European Union (ERDF) and the Free State of Saxony (C2 – 13927/2379).

LITERATURE CITED

Agarwal UP, Reiner RS, Ralph SA. 2010. Cellulose I crystallinity determination using FT-Raman spectroscopy: univariate and multivariate methods. *Cellulose* **17**: 721–733.

Altenbach H, Altenbach J, Rikards R. 1996. *Einführung in die Mechanik der Laminat- und Sandwichtragwerke*, 1st edn. Stuttgart: Deutscher Verlag für Grundstoffindustrie.

Bogart SJ, Spiers G, Cholewa E. 2010. X-ray microCT imaging technique reveals corm microstructures of an arctic–boreal cotton-sedge, *Eriophorum vaginatum*. *Journal of Structural Biology* **171**: 361–371.

Boyd DW, Harris WM, Murry LE. 1982. Sclereid development in Camellia petioles. *American Journal of Botany* **69**: 339–347.

Burgert I, Fratzl P. 2009. Plants control the properties and actuation of their organs through the orientation of cellulose fibrils in their cell walls. *Integrative and Comparative Biology* **49**: 69–79.

Burgert I, Eder M, Gierlinger N, Fratzl P. 2007. Tensile and compressive stresses in tracheids are induced by swelling based on geometrical constraints of the wood cell. *Planta* **226**: 981–987.

Busch S, Seidel R, Speck O, Speck T. 2010. Morphological aspects of self-repair of lesions caused by internal growth stresses in stems of *Aristolochia macrophylla* and *Aristolochia ringens*. *Proceedings of the Royal Society B* **277**: 2113–2120.

Cai Y, Li G, Nie J., *et al*. 2010. Study of the structure and biosynthetic pathway of lignin in stone cells of pear. *Scientia Horticulturae* **125**: 374–379.

Drazeta L, Lang A, Cappellini C, Hall AJ, Volz RK, Jameson PE. 2004. Vessel differentiation in the pedicel of apple and the effects of auxin transport inhibition. *Physiologia Plantarum* **120**: 162–170.

Ennos AR. 2012. *Solid biomechanics*, 1st edn. Princeton, NJ: Princeton University Press.

Eschrich W. 1995. Funktionelle Pflanzenanatomie, *1st edn*. Berlin: Springer.

Evert RF. 1963. Ontogeny and structure of the secondary phloem in *Pyrus malus*. *American Journal of Botany* **50**: 8–37.

Evert RF. 2006. Esau's plant anatomy, *3rd edn*. Hoboken, NJ: Wiley.

Fengel D, Wegener G. 1989. Wood: chemistry, ultrastructure, reactions, *1st edn*. Berlin: Walter de Gruyter.

Franceschi VR, Krokene P, Christiansen E, Krekling T. 2005. Tansley review – Anatomical and chemical defenses of conifer bark against bark beetles and other pests. *New Phytologist* **167**: 353–376.

Ganino T, Rapoport HF, Fabbri A. 2011. Anatomy of the olive inflorescence axis at flowering and fruiting. *Scientia Horticulturae* **129**: 213–219.

Gibson LJ. 2012. The hierarchical structure and mechanics of plant materials. *Journal of the Royal Society Interface* **9**: 2749–2766.

Gierlinger N, Luss S, König C, Konnerth F, Eder M, Fratzl P. 2010. Cellulose microfibril orientation of *Picea abies* and its variability at the micron-level determined by Raman imaging. *Journal of Experimental Botany* **61**: 587–595.

Goswami L, Dunlop JWC, Jungnikl K, *et al*. 2008. Stress generation in the tension wood of poplar is based on the lateral swelling power of the G-layer. *The Plant Journal* **56**: 531–538.

Haigler CH, Weimer PJ. 1991. Biosynthesis and biodegradation of cellulose, *1st edn*. New York: Marcel Dekker.

Harris D, Stork J, Debolt S. 2009. Genetic modification in cellulose-synthase reduces crystallinity and improves biochemical conversion to fermentable sugar. *GCB Bioenergy* **1**: 51–61.

Harris SA, Robinson JP, Juniper BE. 2002. Genetic clues to the origin of the apple. *Trends in Genetics* **18**: 426–430.

Heide-Jorgensen HS. 1990. Xeromorphic leaves of *Hakea suaveolens* R. Br. IV. Ontogeny, structure and function of the sclereids. *Australian Journal of Botany* **38**: 25–43.

Hernandez-Ledesma P, Terrazas T, Flores-Olvera H. 2011. Comparative stem anatomy of *Mirabilis* (Nyctaginaceae). *Plant Systematics and Evolution* **292**: 117–132.

Höfer M, Flachowsky H, Hanke MV., *et al*. 2013. Assessment of phenotypic variation of *Malus orientalis* in the North Caucasus region. *Genetic Resources and Crop Evolution*. **60**: 1463–1477.

James KR, Haritos N, Ades PK. 2006. Mechanical stability of trees under dynamic loads. *American Journal of Botany* **93**: 1522–1530.

Karabourniotis G. 1998. Light-guiding function of foliar sclereids in the evergreen sclerophyll *Phillyrea latifolia*: a quantitative approach. *Journal of Experimental Botany* **49**: 739–746.

Khatun M, Mondal AK. 2011. Studies on the sclereids diversity and distribution pattern in the different plant organs (leaves, stems and fruits) of some selected medicinally viable angiospermic taxa in Eastern India: a systematic approach. *Advances in Bioresearch* **2**: 111–121.

Köhler L, Spatz H-C. 2002. Micromechanics of plant tissues beyond the linear-elastic range. *Planta* **215**: 33–40.

Kölln K. 2004. *Morphology and mechanical characteristics of cellulose fibres. Investigations with X-ray and neutron scattering*. PhD Thesis, Christian-Albrechts-Universität of Kiel, Germany.

Kühlhorn A, Silber G. 2000. *Technische Mechanik für Ingenieure*, 1st edn. Heidelberg: Hüthig Verlags.

Lang A, Ryan KG. 1994. Vascular development and sap flow in apple pedicels. *Annals of Botany* **74**: 381–388.

Leroux O. 2012. Collenchyma: a versatile mechanical tissue with dynamic cell walls. *Annals of Botany* **110**: 1083–1098.

Lion A, Kardelky C. 2004. The Payne effect in finite viscoelasticity: constitutive modelling based on fractional derivatives and intrinsic time scales. *International Journal of Plasticity* **20**: 1313–1345.

Meier U, Graf H, Hack H., *et al*. 1994. Phänologische Entwicklungsstadien des Kernobstes (*Malus domstica* Borkh. und *Pyrus communis* L.) des Steinobstes (*Prunus*-Arten), der Johannisbeere (*Ribes*-Arten) und der Erdbeere (*Fra-garia* × *ananassa* Duch.). *Nachrichtenblatt des Deutschen Pflanzenschutzdienstes* **46**: 141–153.

Mellerowicz EJ, Immerzeel P, Hayashi T. 2008. Xyloglucan: the molecular muscle of trees. *Annals of Botany* **102**: 659–665.

Möller R, Koch G, Nanayakkara B, Schmitt U. 2005. Lignification in cell cultures of *Pinus radiata*: activities of enzymes and lignin topochemistry. *Tree Physiology* **26**: 201–210.

Mondolot L, Roussel JL, Andary C. 2001. New applications for an old lignified element staining reagent. *The Histochemical Journal* **33**: 379–385.

Namikawa I. 1922. Über die vorzeitige Abstossung der jungen Früchte von *Malus communis*. *Journal of the College of Agriculture, Hokkaido Imperial University, Sapporo, Japan* **11**: 1–21.

Newman RH, Hemmingson JA. 1994. Carbon-13 NMR distinction between categories of molecular order and disorder in cellulose. *Cellulose* **2**: 95–110.

Niklas KJ. 1988. Dependency of the tensile modulus on transverse dimensions, water potential and cell number of pith parenchyma. *American Journal of Botany* **75**: 1286–1292.

Niklas K.J. 1989. Mechanical behaviour of plant tissues as inferred from the theory of pressurized cellular solids. *American Journal of Botany* **76**: 929–937.

Niklas KJ. 1992. *Plant biomechanics: an engineering approach to plant form and function*, 1st edn. Chicago: University of Chicago Press.

Niklas KJ, Paolillo DJ. 1998. Preferential states of longitudinal tension in the outer tissues of *Taraxacum officinale* (Asteraceae) peduncles. *American Journal of Botany* **85**: 1068–1081.

Parameswaran N. 1975. On the fine structure on the wall of sclereids in some tree barks. *Protoplasma* **85**: 305–314.

Phipps JB, Robertson KR, Smith PG, Rohrer JR. 1990. A checklist of the subfamily Maloideae (Rosaceae). *Canadian Journal of Botany* **68**: 2209–2269.

Placet V, Trivaudey F, Cisse O, Gucheret-Retel V, Boubakar ML. 2012. Diameter dependence of the apparent tensile modulus of hemp fibres: a morphological, structural or ultrastructural effect? *Composites: Part A* **43**: 275–287.

Prislan P, Koch G, Schmitt U, Gricar J, Cufar K. 2012. Cellular and topochemical characteristics of secondary changes in bark tissues of beech (*Fagus sylvatica*). *Holzforschung* **66**: 131–138.

Rees DWA. 2009. *Mechanics of optimal structural design: minimum weight structures*, 1st edn. Chichester: Wiley.

Reis D, Vian B. 2004. Helicoidal pattern in secondary cell walls and possible role of xylans in their construction. *Comptes Rendus Biologies* **327**: 785–790.

Reutemann AG, Vegetti AC, Pozner R. 2012. Structure and development of the style base in *Abildgaardia*, *Bulbostylis*, and *Fimbristylis* (Cyperaceae, Cyperoideae, Abildgaardieae). *Flora* **207**: 223–236.

Rivero-Maldonado G, Sanchez-Urdaneta A, Quieros de G. M, Sanabria ME, Colmenares C, Ortega J. 2008. Histological alterations caused by *Brevipalpus phoenicis* (Geijskes) to peduncles and sepals of *Psidium guajava* L. *Revista de la Facultad de Agronomía de La Universidad del Zulia* **25**: 525–549.

Robinson JP, Harris SA, Juniper BE. 2001. Taxonomy of the genus *Malus* Mill. (Rosaceae) with emphasis on the cultivated apple, *Malus domestica* Borkh. *Plant Systematics and Evolution* **226**: 35–58.

Roland JC, Reis D, Vian B, Satiat-Jeunemaitre B, Mosiniak M. 1987. Morphogenesis of plant cell walls at the supramolecular level: internal geometry and versatility of helicoidal expression. *Protoplasma* **140**: 75–91.

Romanov MS, Bobrov AVF, Wijesundara DSA, Romanova ES. 2011. Pericarp development and fruit structure in borassoid palms (Arecaceae – Coryphoideae – Borasseae). *Annals of Botany* **108**: 1489–1502.

Rüggeberg M, Burgert I, Speck T. 2009*a*. Structural and mechanical design of tissue interfaces in the giant reed *Arundo donax*. *Journal of the Royal Society Interface* **7**: 499–506.

Rüggeberg M, Speck T, Burgert I. 2009*b*. Structure–function relationships of different vascular bundle types in the stem of the Mexican fanpalm (*Washingtonia robusta*). *New Phytologist* **182**: 443–450.

Savidge RA. 1983. The role of plant hormones in higher plant cellular differentiation. II. Experiments with the vascular cambium, and sclereid and tracheid differentiation in the pine, *Pinus contorta*. *Histochemical Journal* **15**: 447–466.

Schwarz W. 1929. Zur physiologischen Anatomie der Fruchtstiele schwerer Früchte. *Planta* **8**: 185–251.

Sharma M. 1970. A study of brachysclereids in two members of Capparidaceae. *Proceedings of the Indian Academy Part B* **72**: 47–55.

Sivan P, Mishra P, Rao KS. 2010. Occurrence of reaction xylem in the peduncle of *Couroupita guianensis* and *Kigelia pinnata*. *IAWA Journal* **31**: 203–216.

Spatz H-C, Theckes B. 2013. Oscillation damping in trees. *Plant Science* **207**: 66–71.

Sun L, Bukovac MJ, Forsline PL, van Nocker S. 2009. Natural variation in fruit abscission-related traits in apple (*Malus*). *Euphytica* **165**: 55–67.

Theckes B, de Langre E, Boutillon X. 2011. Damping by branching: a bioinspiration from trees, *Bioinspiration and Biomimetics* **6**: 046010.

Thielen M, Speck T, Seidel R. 2013. Viscoelasticity and compaction behaviour of the foam-like pomelo (*Citrus maxima*) peel. *Journal of Materials Science* **48**: 3469–3478.

Wacker R. 2006. Eine neue einfache Methode zur polychromatischen Anfärbung von Paraffinschnitten pflanzlicher Gewebe für Durchlicht- und Fluoreszenzmikroskopie. *Mikrokosmos* **4**: 210–212.

Wrana C, Fischer C, Härtel V. 2003. Dynamic measurements on filled elastomers by mono- and bimodal excitations. *Kautschuk, Gummi, Kunststoffe* **9**: 437–443.

Wu L, Joshi CP, Chiang VL. 2000. A xylem-specific cellulose synthase gene from aspen (*Populus tremuloides*) is responsive to mechanical stress. *The Plant Journal* **22**: 495–502.

Zhang W, Wang XQ, Li ZY. 2010. The protective shell: sclereids and their mechanical function in corollas of some species of *Camellia* (Theaceae). *Plant Biology* **13**: 688–692.